ACS Energy LETTERS

Cite This: ACS Energy Lett. 2019, 4, 968–976

http://pubs.acs.org/journal/aelccp

LETTER

Decoupling $H_2(g)$ and $O_2(g)$ Production in Water Splitting by a Solar-Driven $V^{3+/2+}(aq,H_2SO_4)|KOH(aq)$ Cell

Alec Ho,[†] Xinghao Zhou,[‡] Lihao Han,[†] Ian Sullivan,[†] Christoph Karp,[†] Nathan S. Lewis,*[,†,§,∥] and Chengxiang Xiang*[,†]

[†]Division of Chemistry and Chemical Engineering, California Institute of Technology, Pasadena, California 91125, United States

[‡]Division of Engineering and Applied Science, Department of Applied Physics and Materials Science, California Institute of Technology, Pasadena, California 91125, United States

[§]Beckman Institute Molecular Materials Research Center, California Institute of Technology, Pasadena, California 91125, United States

[∥]Kavli Nanoscience Institute, California Institute of Technology, Pasadena, California 91125, United States

Supporting Information

ABSTRACT: A solar-driven $V^{3+/2+}(aq,H_2SO_4)|KOH(aq)$ cell, consisting of a carbon-cloth cathode in 2.0 M $H_2SO_4(aq)$ with 0.36 M $V_2(SO_4)_3$ (pH −0.16), a Ni mesh anode in 2.5 M KOH(aq) (pH 14.21) for the oxygen-evolution reaction (OER), and a bipolar membrane that sustained the pH differentials between the catholyte and anolyte, enabled water splitting with spatial and temporal decoupling of the hydrogen evolution reaction (HER) from the OER and produced $H_2(g)$ locally under pressure upon demand. Over a range of potentials and charging depths, V^{3+} was selectively reduced with >99.8% faradic efficiency. The V^{2+} species produced in the catholyte was then passed subsequently on demand over a MoC_x-based HER catalyst to produce $H_2(g)$ and regenerate V^{3+} for subsequent reduction. Under a base hydrogen pressure of 1, 10, and 100 atm, the discharge efficiency of the V^{3+} to hydrogen was 83%, 65.2%, and 59.8%, respectively. In conjunction with a solar tracker and a photovoltaic device, the $V^{3+/2+}(aq,H_2SO_4)|KOH(aq)$ cell was charged outdoors under sunlight and discharged at night with a daily averaged diurnal solar-to-hydrogen (STH) energy conversion efficiency of 3.7% and a STH conversion efficiency of 5.8% during daylight operation.

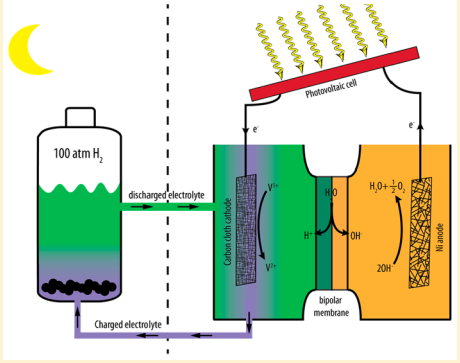

In a solar-driven water-splitting electrochemical cell, the hydrogen-evolution reaction (HER) occurs at the cathode while the oxygen-evolution reaction (OER) occurs at the anode:[1]

HER in acidic solution:

$$2H^+ + 2e^- \rightarrow H_2 \quad (E^\circ = -244 \text{ mV vs SCE}) \tag{1a}$$

HER in alkaline solution:

$$2H_2O + 2e^- \rightarrow H_2 + OH^- \quad (E^\circ = -1074 \text{ mV vs SCE}) \tag{1b}$$

OER in acidic solution:

$$2H_2O \rightarrow O_2 + 4H^+ + 4e^- \quad (E^\circ = 986 \text{ mV vs SCE}) \tag{2a}$$

OER in alkaline solution:

$$4OH^- \rightarrow O_2 + 2H_2O + 4e^- \quad (E^\circ = 156 \text{ mV vs SCE}) \tag{2b}$$

where SCE is the standard calomel electrode in saturated KCl. In a phototelectrochemical (PEC) cell, reactions 1 and 2 are tightly coupled, and to ensure charge neutrality, they must proceed at the same rate.[2−5] Hence, most solar-driven water-splitting cells, operated either under conventional single-electrolyte conditions[5,6] or in electrolytes that have sustained pH differentials between the catholyte and anolyte,[3,4] generate $H_2(g)$ and $O_2(g)$ simultaneously in the cell, so that whenever one oxygen molecule is produced at the anode, two hydrogen molecules are produced at the cathode. $H_2(g)/O_2(g)$ mixtures

Received: February 4, 2019
Accepted: March 21, 2019
Published: March 21, 2019

DOI: 10.1021/acsenergylett.9b00278
ACS Energy Lett. 2019, 4, 968−976

have a flammability limit of 4 vol % and an explosive limit of 15 vol %;[7] therefore, for safety purposes, membrane separators such as a cation-exchange membrane (CEM), e.g., Nafion, an anion-exchange membrane (AEM), e.g., Selemion, or a bipolar membrane (BPM), e.g., Fumasep, are often used to support ionic transport and prevent gaseous-product crossover.[2,3] Membrane-free devices lack a robust mechanism to prevent product-gas crossover, and in some measurements, up to 40% of H_2 is present in the O_2-containing anolyte chamber;[8] however, in some cases, strategies have been developed to separate the products under 1 atm of pressure with low crossover rates.[9,10] The membrane separator also facilitates the production of $H_2(g)$ under pressure by electrochemical processes.[11,12]

Membrane separators provide an effective method to minimize product crossover, but mechanical failures and pinhole formation in the membrane introduce safety concerns.[13,14] Additionally, such an approach necessitates a balance-of-systems for collection of the evolved $H_2(g)$ over large areas as well as pressure management technologies associated with accommodating the time-varying instantaneous intensity of sunlight striking the system at different spatial locations.[2,3,6] An approach that enabled the separate generation of hydrogen and oxygen in space and time would thus entail several advantages, including mitigating the concern related to production of potentially flammable or explosive gas mixtures. In such an approach, the hydrogen generation rate could also beneficially be decoupled from, and thus could substantially exceed, the rate of generation of energetic electrons and holes in the illuminated light absorbers. Furthermore, the H_2 could be formed upon demand under pressure at a specific desired location. A benign aqueous solution could constitute the redox catholyte material collected over the large solar-illuminated area and serve as the collected energy carrier, with the $O_2(g)$ produced in place and vented to the atmosphere without the presence of $H_2(g)$ at that location.

Two general strategies have been used to decouple the HER and OER electrochemically and/or photoelectrochemically. The first strategy involves a two-step electrolysis, in which the water-splitting reaction is effected in two physically distinct, separate electrochemical cells, using redox species or redox electrodes such as NiOOH electrodes,[15,16] a polytriphenylamine-based battery electrode,[17] or molecular electron-coupled-proton buffers.[18,19] The second strategy to decouple the generation of hydrogen and oxygen involves a (photo)-electrochemical process in conjunction with a subsequent chemical process, using for example silicotungstic acid,[20] vanadium, or cerium redox couples[21] as electrochemical mediators to couple two electrochemical processes and allow completion of a sustainable, complete water-splitting process.

Herein, we demonstrate such a spatially and temporally decoupled approach to solar-driven electrochemical water-splitting, in which the electrons and protons generated during the OER are used to charge an aqueous $V^{3+/2+}(aq)$ solution in 2.0 M sulfuric acid (pH −0.16) (reaction 3), rather than being used directly to produce $H_2(g)$ at the cathode. The protons produced at the anode are transported to the catholyte and temporarily stored in the catholyte, which causes the decrease of the catholyte pH during the charging process.

$$V^{3+} + e^- \rightarrow V^{2+} \quad (E^{o\prime} = -0.499\ \text{V vs SCE}) \tag{3}$$

To produce $H_2(g)$ from water, the catholyte that contains the V^{2+} is then exposed upon demand, if desired at a separate location and time, to a catalyst in the dark. During the chemical discharging process, the pH of the catholyte increases back to its initial value upon the release of hydrogen. In the demonstration system developed herein, the charged vanadium solution V^{2+} is specifically contacted with a Mo_2C catalyst, resulting in the production of $H_2(g)$ and V^{3+} (reaction 4).

$$2H^+ + 2\,V^{2+} \xrightarrow{Mo_2C} H_2 + 2\,V^{3+} \tag{4}$$

The full cell, and thus the overall water-splitting process, is completed with the evolution of $O_2(g)$ from water at the anode, as per equation 2a or 2b.

The $V^{3+/2+}$ redox couple is however soluble only in acidic conditions, in which a stable, active, earth-abundant OER catalyst has yet to be discovered.[22,23] A range of OER catalysts composed of binary, ternary, or quaternary metal oxides exhibit low overpotentials and high stabilities in alkaline conditions.[24−27] To simultaneously accommodate the optimal pH conditions for the OER and vanadium redox reactions, a bipolar membrane has thus been used in the demonstration system discussed herein, to sustain the pH differential between the cathode and the anode chamber under steady-state operation in the cell as well as to enable the use of earth-abundant electrocatalysts in a system that produces $H_2(g)$ locally under pressure and upon demand. Figure S1 shows a schematic illustration of the full process flow.

Figure 1 shows a schematic illustration of the solar-driven $V^{3+/2+}(aq, H_2SO_4)|KOH(aq)$ system, which for proof-of-concept purposes consisted of a series connection between a photovoltaic module and an electrochemical cell. The 16.0% efficient polycrystalline Si photovoltaic module produced the photovoltage and photocurrent necessary to drive the electrochemical reactions, although an analogous process could occur in an integrated system that used instead a photoelectrode either as the anode, cathode, or both.[28−30] For example, in conjunction with appropriately selected photoanodes, p-InP and p-Si could be used in an integrated system, because both materials provide stable photocathodes in contact with $V^{3+/2+}(aq)$-HCl(aq) with p-InP exhibiting >11% efficiency under such conditions.[31] A carbon cloth electrode effected the reduction of vanadium in 2.0 M H_2SO_4 (pH −0.16), with an initial $[V^{3+}] = 0.36$ M; a Ni mesh electrode performed the OER in 2.5 M KOH (pH 14.21), and a bipolar membrane sustained the pH differentials and provided protons and hydroxide ions to the catholyte and anolyte, respectively.

The electrochemical behaviors of the cathode, anode, and bipolar membrane were evaluated separately (Figure 2). Figure 2a shows the liner sweep voltammetry, at a scan rate of 40 mV s^{-1}, of a Ni mesh electrode in 2.5 M KOH(aq) (pH 14.21) (red) and of a Pt foil electrode in 1.0 M H_2SO_4(aq) (blue). Under these conditions, an overpotential of 379 mV, i.e., a potential of 539 mV vs SCE, was required for the Ni mesh to drive the OER at an anodic geometric current density of 10 mA cm^{-2}. The relatively low current density, 10 mA cm^{-2}, was chosen for evaluating the catalyst and cell performance because of the relatively low photon flux from sunlight for the potential usage of this proof-of-concept device in a distributed system. Figure 2b shows the voltammetry, at a scan rate of 40 mV s^{-1}, of a carbon cloth electrode in a 2.0 M H_2SO_4(aq) with (green) and without 0.36 M $V_2(SO_4)_3$ (black). A potential of −765 mV vs SCE, i.e., an overpotential of −266 mV relative to $E^{o\prime}(V^{3+/2+})$, was required to drive the V^{3+} reduction at a cathodic geometric current density of 10 mA cm^{-2}. In contrast, at the same current density in the pure 2.0 M H_2SO_4(aq) solution, a potential of

DOI: 10.1021/acsenergylett.9b00278
ACS Energy Lett. 2019, 4, 968−976

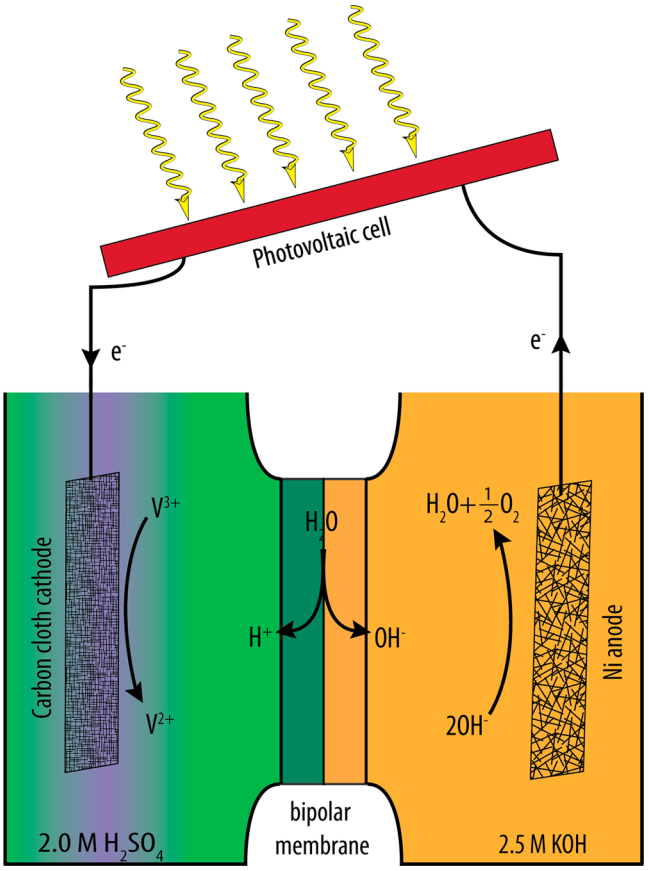

Figure 1. Schematic illustration of a solar-driven $V^{3+/2+}$(aq,H_2SO_4)| KOH(aq) cell in which a photovoltaic module generates energetic electrons and holes, a carbon cloth cathode effects vanadium reduction in 2.0 M H_2SO_4(aq), a Ni mesh anode oxidizes water to O_2(g) in 2.5 M KOH(aq), and a bipolar membrane sustains the pH differential between the cathode and anode chambers.

−858 mV vs SCE, i.e., an overpotential of −614 mV, was required to drive the HER. During the vanadium redox charging process, HER is a parasitic side reaction, which is suppressed because of the slow kinetics for the HER at carbon cloth electrodes.

The polarization behaviors of the bipolar membrane that sustained the pH differentials between the catholyte and anolyte with or without the vanadium redox couples were measured in the absence of, and then in the presence of, the vanadium redox couples. Figure 2c shows the voltage drop measured with a four-point configuration across the bipolar membrane, as a function of the current density normalized to the area of the bipolar membrane. The gray polarization curve represents the electrolyte combination of KOH(aq) (pH 14.21) and 2.0 M H_2SO_4(aq) (pH −0.16) without the vanadium redox species. A slight decrease in the voltage loss was observed when 0.36 M $V_2(SO_4)$ was added to the catholyte (black polarization curve, Figure 2c), likely because of the increased conductivity of the solution due to the presence of additional electrolyte. At open-circuit, the equilibrium potential drop, $V_{membrane,equilibrium}$ was 0.059(14.21 + 0.16) = 0.848 V. At a current density of 10 mA cm^{-2}, the potential difference across the bipolar membrane was 0.866 V in the presence of $V^{3+/2+}$. The bipolar membrane voltage loss at 10 mA cm^{-2} was therefore $V_{membrane,loss} = V_{membrane,total} - V_{membrane,equilibrium}$ = 0.866 V − 0.848 V = 0.018 V. The observed current-voltage characteristic of the bipolar membrane at two extreme pH values is in agreement with prior reports[32,33] and is substantially lower than voltage losses across bipolar membranes operated in near-neutral pH conditions.[3,33−36] Table S1 summarizes the voltage losses in the reported bipolar membrane systems. At two extreme pH values, the minimal voltage loss across the bipolar membrane[33,37] is consistent with the hypothesis that no additional Donnan potential drop is present across the membrane/electrolyte interface, and all the electric field drops primarily occur at the CEM and AEM interface. The voltage stability and the crossover properties of the bipolar membrane were also measured. Figure 2d shows the voltage measured across the bipolar membrane as a function of time, when the 0.36 M $V_2(SO_4)_3$, 2.0 M H_2SO_4(aq) (pH −0.16)/ bipolar membrane/2.5 M KOH(aq) (pH 14.21) cell was biased at a constant current density of 10 mA cm^{-2}. These data indicated negligible degradation in the voltage across the bipolar membrane over the course of a 200 h stability test. For >200 h, the bipolar membrane remained stable, and no precipitate was observed either in the bipolar membrane or in the anolyte. The geometric surface areas of the bipolar membrane, carbon cathode, and nickel mesh anode were all 6.0 cm^2. To study the ion crossover behaviors, the concentrations of $V^{3+/2+}$ in the anolyte before and after continuous operation at 10 mA cm^{-2} for 24 h were determined using inductively coupled plasma mass spectroscopy (ICP-MS, Table S2), and the concentrations of K^+ in the catholyte and SO_4^{2-} in the anolyte were determined using ion chromatography (IC). Table 1 lists the transport current density corresponding to the leakage of $V^{3+/2+}$, K^+, and SO_4^{2-} across the membrane when the cell was operated at 10 mA cm^{-2}. The membrane selectivity in the absence of and then in the presence of vanadium species, determined by the ratio of the proton-carried and hydroxide-carried portions of the total passed charges, f_{H^+} and f_{OH^-}, is also summarized in Table 1. The $V^{3+/2+}$ crossover current density was negligible partly because of the electric field lines during the cell operation repelling the positively charged vanadium redox species from entering the bipolar membrane and the anolyte. The presence of $V^{3+/2+}$ also did not substantially affect membrane selectivity. Both the f_{H^+} and f_{OH^-} values exceeded 92% at an operating current density of 10 mA cm^{-2}, in accord with prior results.[3]

The electrochemical charging and discharging behaviors of the carbon cloth electrode in $V^{3+/2+}$, 2.0 M H_2SO_4(aq) were then investigated. Figure 3a shows the experimental (red) and theoretical (blue) decay of the current density with respect to charge passed into a 0.36 M $V_2(SO_4)_3$, 2.0 M H_2SO_4 solution. To obtain the current density ascribable to V^{3+} reduction (Figure 3a, red), the current density that effected H_2(g) production (black) was subtracted from the overall current density, with the average H_2(g)-related current density over 30 min intervals calculated by measurement of the amount of H_2(g) collected with respect to charge passed. The decrease in current density as a function of charge passed followed the trend expected from the Nernst relation (eq 5), where k is Boltzmann's constant, T the absolute temperature, e the unsigned charge on an electron, E the Nernstian cell potential, $E^{\circ\prime}$ the formal potential, [Red] the concentration of reduced species, and [Ox] the concentration of oxidized species.

$$E = E^{\circ\prime} - \frac{kT}{q}\ln\frac{[\mathrm{Red}]}{[\mathrm{Ox}]} \quad (5)$$

The initial rapid decay of the current density was due to the rapid change of $E(V^{3+/2+})$ (eq 2). As $[V^{3+}]$ decreased and $[V^{2+}]$

DOI: 10.1021/acsenergylett.9b00278
ACS Energy Lett. 2019, 4, 968−976

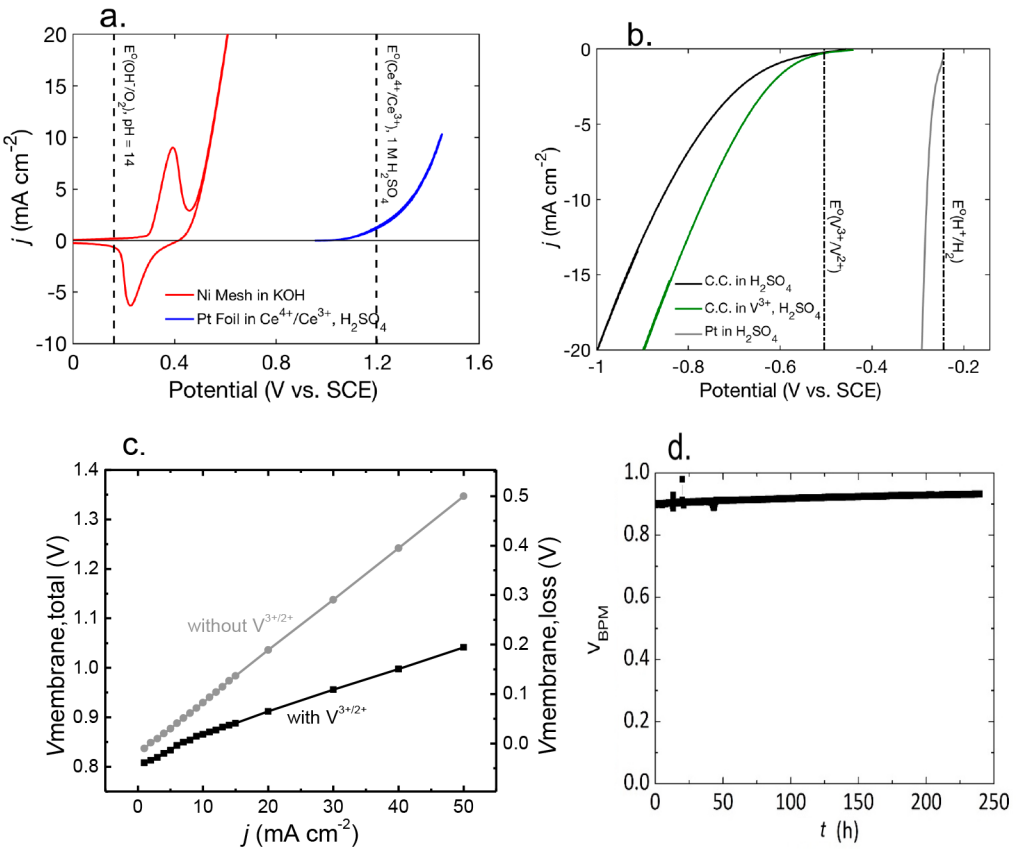

Figure 2. (a) Voltammetry of a Ni mesh (6.0 cm^2 geometric area) in 2.5 M KOH(aq) (red) and Pt foil (0.12 cm^2 area) in Ce^{4+}/Ce^{3+}, 1.0 M H_2SO_4(aq) (blue). (b) Voltammetry of a carbon cloth in 2.0 M H_2SO_4 (black) as well as of carbon cloth (6.0 cm^2 geometric area) in 0.36 M V^{3+}, 2.0 M H_2SO_4(aq) (green). For comparison, voltammetry of Pt in 1.0 M H_2SO_4(aq) (gray) is shown.[40,41] (c) Measured membrane voltage and voltage loss with (black squares) and without (gray circles) the presence of vanadium species, as a function of the current density normalized to the bipolar membrane. The cell configuration was 2.0 M H_2SO_4(aq) (pH −0.16) with or without V^{3+} /V^{2+}/BPM/KOH(aq) (pH 14.21). (d) Bipolar membrane voltage as a function of time, with the current density across the bipolar membrane maintained at 10 mA cm^{-2}. The BPM, cathode, and anode each had a geometric surface area of 6.0 cm^2.

Table 1. Ion Crossover Rates for the Bipolar Membrane in the Absence and Then in the Presence of Vanadium Ions

$J_{Membrane}$ = 10 mA cm^{-2}	$J_{V3+/2+}$	J_{K+} (μA cm^{-2})	$J_{SO_4^{2-}}$ (μA cm^{-2})	f_{H^+}	f_{OH^-}
with $V^{3+/2+}$	0.226 μA cm^{-2}	787	54	92.1%	99.5%
without $V^{3+/2+}$	N.A.	606	184	93.9%	98.2%

increased linearly as a function of the charge passed, the Nernstian cell potential shifted logarithmically to more negative values, consistent with the observed decreases in the charging current (Figure 3a). The pH of the catholyte, an aqueous $V^{3+/2+}$(aq) solution in 2.0 M sulfuric acid, of the hybrid solar-driven water-splitting system decreased during the charging process and increased back to its initial value during the discharging process. The change of the pH in the reported system is small (from −0.16 to −0.30) because of the large concentration differential between the redox species and the sulfuric acid, and consequently the pH change had minimal effects on the catalytic activities of the redox species or on the efficiency of the device.

Figure 3b shows the collected H_2(g) as a function of the charge passed for the carbon cloth cathode at −730 mV (purple), −830 mV (green), and −1000 mV (blue) vs SCE in 0.36 M $V_2(SO_4)_3$, 2.0 M H_2SO_4(aq). Before the charging capacity of the electrolyte was reached at each different potential, negligible H_2(g) was produced during charging of the 50.0 mL $V^{3+/2+}$(aq) solution. In contrast, as expected, a linear increase of the collected H_2(g) production (red) as a function of the charge passed was observed for the same carbon cloth electrode in the blank 2.0 M H_2SO_4(red) (dotted black line). For the carbon cloth electrode at −830 mV or at −1000 mV vs SCE, after the vanadium electrolyte reached its charging capacity, a rapid switch to H_2(g) production was observed, with a rate of H_2(g) generation matching the theoretical value. When the carbon cloth electrode was poised at −730 mV vs SCE, an increase in the rate of H_2(g) production began at ∼83% of the $V^{3+/2+}$ charging capacity. The operating current density decreased substantially, to ∼0 mA cm^{-2}, for the low-overpotential condition (−730 mV vs SCE), whereas before reaching its charging capacity (see Figure S2), the operating cathodic current density remained above ∼0.8 and ∼2.5 mA cm^{-2} for the high-overpotential conditions, −830 and −1000 mV, respectively. Hence, during charging, the shifts in the equilibrium potential for the vanadium electrolyte resulted in the decrease in operating current density (Figure 3a) and decreased the selectivity toward vanadium reduction. To achieve near-unity faradic efficiency (FE) for vanadium reduction, an overpotential of 331 mV, or a potential of −830 mV vs SCE, was required during the reaction.

DOI: 10.1021/acsenergylett.9b00278
ACS Energy Lett. 2019, 4, 968−976

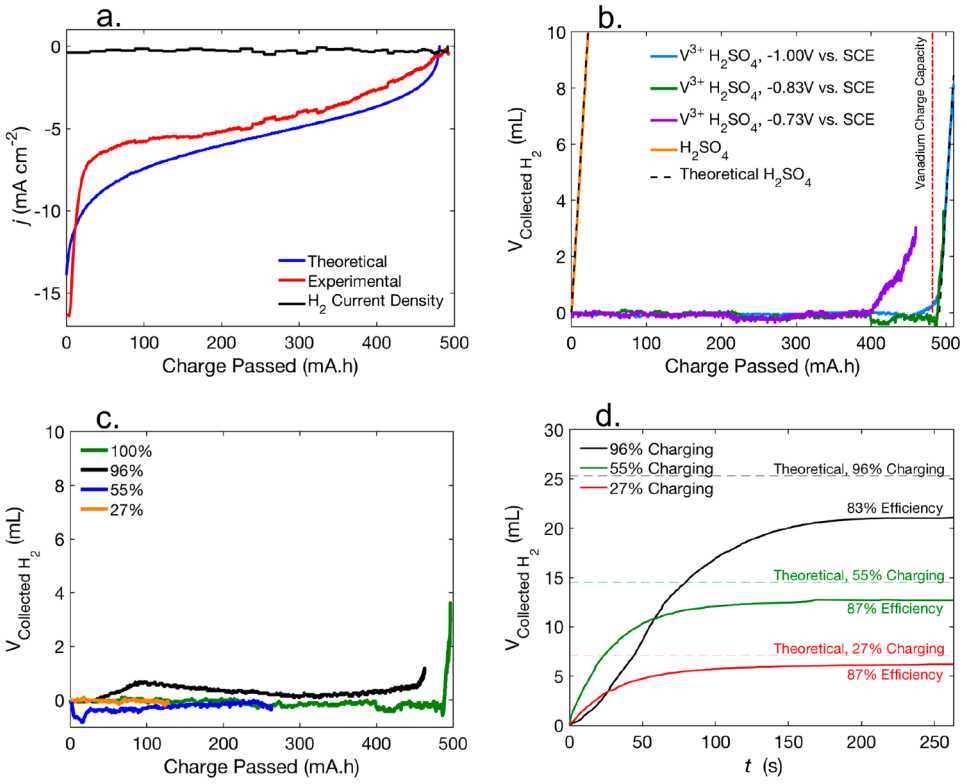

Figure 3. (a) Partial current density for the reduction of 0.36 M V^{3+} in 2.0 M H_2SO_4(aq) at −830 mV (vs SCE) (red), partial current density for production of H_2(g) (black), and the theoretical current density determined by the Nernst equation, accounting for the 10 mA·h passed to the solution during the voltammetry (blue). (b) Measured H_2(g) collection during cell operation for 2.0 M H_2SO_4 (aq) (orange), 0.36 M V^{3+} in 2.0 M H_2SO_4(aq) at −1.00 V (blue), −0.830 V (green), and −0.73 V (purple) vs SCE, respectively. The dotted black line shows the expected H_2 production volume in 2.0 M H_2SO_4 in the absence of vanadium species. (c) Hydrogen produced during runs of varying charge capacities at −830 mV vs SCE. (d) Measured H_2(g) collection during reaction of 6.0 mL of partially reduced 0.36 M V^{2+}, 2.0 M H_2SO_4 in the presence of the Mo_2C catalyst.

The collected H_2(g) as a function of the charge passed for the carbon cloth electrode at −830 mV vs SCE, at three different charging depths, is presented in Figure 3c. The carbon cloth electrode exhibited near-unity FE for vanadium reduction at charge capacities of 27% (orange), 55% (blue), and 96% (black), as well as past 100% (green). The highly selective reduction of V^{3+} to V^{2+}, relative to H_2(g) formation, resulted from the competition between the thermodynamic potential of the HER and the kinetic overpotential for vanadium reduction. Although at pH −0.16, E° (H^+/H_2) is 255 mV > $E^{\circ\prime}$($V^{3+/2+}$), carbon cloth is a poor electrocatalyst for the HER, leading to near-unity FE for the vanadium reduction even at potentials substantially more negative than E° (H^+/H_2). In addition, the HER was suppressed substantially when the electrode was biased at the same potential (−830 mV vs SCE) in the electrolyte with the presence of vanadium redox couples (Figure 2b). From the voltammetric behavior (the black and the green curves in Figure 2b) of the electrodes, the differential current densities at −830 mV vs SCE suggest only ∼40% FE for vanadium reduction,; however, near-unity FE was observed at various charging conditions. The absorption of vanadium species at the carbon cloth electrode is likely to play a role in suppressing the HER. During the entire charging process, the expected pH changes were observed in the catholyte. The stored reducing equivalents in V^{2+} can however be rapidly and efficiently converted into H_2(g) by the Mo_2C catalyst (see Figure S4 for experimental setup). Accordingly, H_2(g) production efficiencies (based on the total amount of charge passed) of 87%, 87%, and 83% were observed for vanadium solutions that were charged to 27%, 55%, and 96% of their charging capacity, respectively (Figure 3d), when the produced H_2(g) was vented to the atmosphere. The H_2(g) production efficiencies were defined by the following equation:

$$\eta_{H_2} = \frac{nF(V_{\text{collected\_H}_2}/V_m)}{Q} \quad (6)$$

where n is the number of electrons, F Faraday's constant, $V_{\text{collected\_H}_2}$ the volume of the collected H_2 (mL), V_m the molar volume of gas, and Q the total quantity of electric charge passed during the charging process. The Mo_2C catalyst can be readily filtered through the discharged electrolyte, facilitating catalyst recycling and reuse.

Discharging of the V^{2+} electrolyte was also performed under elevated pressures in a pressurized stainless-steel apparatus (Figures S5 and S6). The apparatus consisted of 10.4 mL of headspace and 25.0 mL of fully charged V^{2+} electrolyte, as well as the Mo_2C catalyst. The pressure of the headspace was equilibrated at 10.0 atm or at 100.0 atm with hydrogen gas. Upon contact of the charged $V^{3+/2+}$ solution with the Mo_2C catalyst, the pressure of the headspace increased rapidly because of the production of H_2(g). At 10.0 and 100.0 atm base pressure, the discharge of the V^{2+} electrolyte increased the pressure of the headspace by 6.65 and 5.97 atm, respectively, corresponding to H_2(g) production efficiencies of 65.2% and 59.8%, respectively.

The electricity-to-fuel conversion efficiency of the bipolar membrane-based hybrid system (Table 2, system C), in which

DOI: 10.1021/acsenergylett.9b00278
ACS Energy Lett. 2019, 4, 968−976

Table 2. Comparison of Conversion Efficiencies of Three Different Systems

	system A[a]	system B[b]	system C[c]
thermodynamic voltage	1.230 V	1.698 V	1.488 V
ideal conversion efficiency	100%	72%	83%
realistic conversion efficiency	72%	52%	54%

[a]System A: Pt/1.0 M H_2SO_4/Nafion/1.0 M H_2SO_4/IrO_x. [b]System B: Carbon cloth/2.0 M H_2SO_4 0.36 M $V_2(SO_4)_3$/Nafion/1.0 M H_2SO_4 0.10 M Ce^{3+}/Pt. [c]System C: Carbon cloth/2.0 M H_2SO_4 0.36 M $V_2(SO_4)_3$/BPM/2.0 M KOH/Ni mesh.

the cathode operated in an acidic solution for vanadium reduction and the anode effected the OER in an alkaline electrolyte, was compared to the behavior of two previously reported systems (Table 2, system A or system B) for hydrogen production at 1 atm. The electricity-to-fuel conversion efficiency of those systems was defined by the following equation:

$$\eta_{\text{electricity-to-fuel}} = \frac{V_{\text{thermodynamic}}}{V_{\text{operating}}} \quad (7)$$

System A is a conventional, direct water-splitting reactor in 1.0 M H_2SO_4(aq), in which the Pt cathode and the IrO_x anode are separated by a Nafion membrane. System B consists of a previously reported indirect water-splitting reactor in which the carbon cloth cathode for vanadium reduction and a Pt anode for Ce oxidation (reaction 8) are separated by a Nafion membrane, with the anolyte and catholyte both at the same pH, i.e., 1.0 M H_2SO_4(aq).[21]

$$Ce^{3+} \rightarrow Ce^{4+} + e^- \quad (E^{\circ\prime} = 1.72 \text{ V vs SCE}) \quad (8)$$

In system B, the reduced vanadium electrolyte and the oxidized cerium electrolyte can be discharged separately to produce H_2(g) (reaction 4) and O_2(g) (reaction 9), respectively.[21]

$$2H_2O + 4Ce^{4+} \xrightarrow{RuO_2} O_2 + 4H^+ + 4Ce^{3+} \quad (9)$$

Table 2 presents the total voltage required for operation under the thermodynamic limit for each of the three systems under consideration. The value of $E^{\circ\prime}(V^{3+/2+})$ is 255 mV more negative than $E^{\circ}(H^+/H_2)$, whereas $E^{\circ\prime}(Ce^{4+/3+})$ is 490 mV more positive than $E^{\circ}(O_2/H_2O)$. Hence, at the thermodynamic limit, the required voltage for system B is 745 mV larger than for system A, and the required voltage for system C is 255 mV more than for system A. Assuming that H_2(g) under standard conditions is the final product for all three systems, the ideal electricity-to-hydrogen conversion efficiencies for system B and system C are therefore 1.230 V/1.698 V = 72%, and 1.230 V/1.488 V= 83%, respectively.

To facilitate comparisons between the three systems operating under realistic conditions, Figure 2 also displays the behavior of a state-of-the-art Pt electrode for the HER as well as for the oxidation of Ce^{3+} oxidation in acid. The state-of-the-art Pt electrode (gray curve in Figure 2b) exhibited a small overpotential (37 mV) at a current density of −10 mA cm^{-2} for the HER. The larger overpotential for V^{3+} reduction at the carbon-cloth electrode (266 mV at −10 mA cm^{-2}, see Table S3) relative to the state-of-the-art HER performance at Pt produces a loss in efficiency in this indirect solar-driven water-splitting system and is likely due to the electrolyte resistive loss in a large geometric area electrode (6.0 cm^2) operating at high currents, which could be further minimized through cell engineering. To drive cerium oxidation (reaction 5) at 10 mA cm^{-2} (blue curve in Figure 2a) at Pt, a potential of 1684 mV vs SCE, i.e., an overpotential of 244 mV, was required. These overpotentials (see Table S3) yield practical electricity-to-hydrogen conversion efficiencies for system B and system C of 52% and 54%, respectively. In addition to the higher attainable electricity-to-fuel conversion efficiency, system C also mitigates the need for noble-metal catalysts, such as RuO_2 in a heated environment, which also entails limited stability for oxygen generation from the Ce^{4+} solution.[21] Note that these efficiency values include losses associated with a lack of equilibration of H_2 under pressure with the charged vanadium solution but neglect the generally small losses associated with energy required to circulate the electrolyte.

This hybrid solar-driven water-splitting system represents a proof-of-concept demonstration of a strategy[20,21] for decoupling HER and OER in which a (photo)electrochemical process is followed by a chemical process, separated in space and time, to produce hydrogen. In traditional PEC systems, generation of pressurized hydrogen over large areas can be challenging because of issues associated with light management, reactant/product flows, etc. This hybrid system also enables the (photo)electrochemical pressurization of hydrogen, using the vanadium redox couple as a mediator to store pressurized hydrogen in a liquid electrolyte. A similar concept has been reported previously using a two-electron, two-proton mediator, silicotungstic acid, for hydrogen generation.[18] In contrast, the hybrid system described herein additionally utilized a bipolar

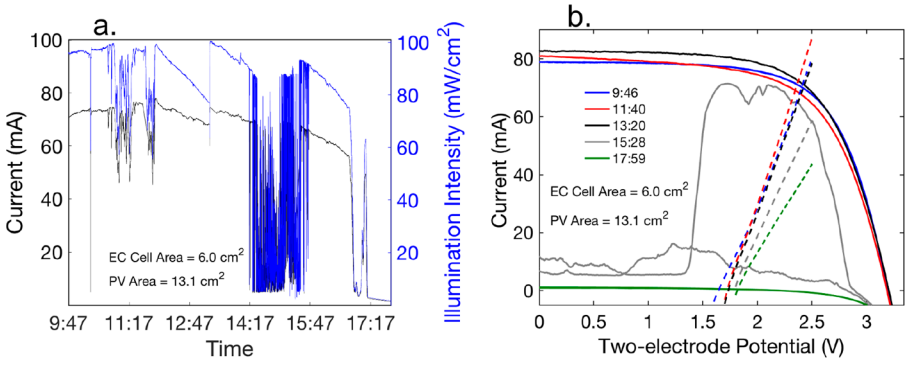

Figure 4. Outdoor measurements. (a) Current of the $V^{3+/2+}$(aq,H_2SO_4)|KOH(aq) cell coupled to a photovoltaic module (black), with the illumination intensity during cell operation measured by a photodiode (blue). (b) Overall polarization behavior for the photovoltaic module (solid lines) and for the $V^{3+/2+}$(aq,H_2SO_4)|KOH(aq) cell (dashed lines) during charging at times in the day.

DOI: 10.1021/acsenergylett.9b00278
ACS Energy Lett. 2019, 4, 968−976

membrane to mitigate the use of precious materials, such as Pt, Ir, or Ru, for the water-oxidation reaction. In contrast to a two-step electrolysis system, in which the water-splitting reaction is effected in two physically distinct, separate electrochemical cells using redox species or redox electrodes,[14,15,17−19] the hybrid approach demonstrated herein is likely to have lower capital costs because only one electrolysis unit, and the associated balance of systems, is required.

To demonstrate the capability of this system to produce spatially and temporally separated streams of $O_2(g)$ and $H_2(g)$, the $V^{3+/2+}(aq,H_2SO_4)|KOH(aq)$ cell with a 6.0 cm^2 electrode area was connected in series with a 16% efficient, 13.1 cm^2 polycrystalline photovoltaic module attached to a solar tracker, and the whole apparatus was tested outdoors (see Figure S3 for picture of the outdoor setup). Figure 4a shows the illumination intensity (blue) and system current (black) for operation during a day. For the first ∼4.5 h, the photocurrent fluctuated around 73 mA, while the illumination intensity fluctuated around 95 mW cm^{-2}. The fluctuations in the photocurrent matched corresponding fluctuations in illumination intensity that were produced by environmental factors. Between 14:17 and 15:47, a wind-blown tree caused extreme variability in the illumination intensity, decreasing it from 95 to ∼5 to mW cm^{-2}, and consequently producing a reduction in the photocurrent from 69 mA to 5.0 mA. Cloud cover between 16:45 and 17:00 caused the illumination intensity to drop to ∼5 mW cm^{-2} and the photocurrent to drop to ∼5.0 mA. After 17:17, a building blocked the photovoltaic module from illumination by direct sunlight, so the illumination intensity decreased to <3 mW cm^{-2}, causing the current to decrease to <3.0 mA. Figure 4b overlays the polarization behavior of the stand-alone $V^{3+/2+}(aq,H_2SO_4)|KOH(aq)$ cell with the current density vs voltage ($J-V$) behavior of the photovoltaic module at various points in the day. As the $V^{3+/2+}$ solution was charged during the outdoor measurements, the polarization data shifted to higher overpotentials and lower current densities, in accordance with the Nernst equation (eq 5). Shifts in the $J-V$ and polarization behavior together caused the photocurrent to vary during operation. After charging to 85% capacity, the entire 50 mL of catholyte was discharged with Mo_2C, producing $H_2(g)$ at 80% overall faradaic efficiency based on the total charge passed. The discharged solution was then filtered with successively smaller filters, and the solution was reused in the system. After the reused solution was charged to 86% capacity, the whole solution was discharged and produced $H_2(g)$ at 78% overall faradaic efficiency based on the total charge passed in the second $V^{3+/2+}$ charging process. In this second charging step, the presence of Mo_2C particles <0.2 μm in size catalyzed the parasitic HER side reaction during charging, leading to a small drop in efficiency in the reused catholyte. Increases in the catalyst size, or using an additional smaller filter, would likely be beneficial to recycling the system. Consistently, charging a fresh vanadium solution to 66% capacity yielded $H_2(g)$ at 84% overall faradaic efficiency based on the total charge passed in this first new charging cycle.

Two efficiency values, a diurnal averaged STH conversion efficiency, $\eta_{diurnal}$, and an average STH conversion efficiency during daylight operation, $\eta_{operating}$, were used to evaluate the performance of the PV-coupled hybrid device. $\eta_{diurnal}$ was defined as $\frac{LVH_{H_2} m_{H_2}}{(DNI_{diurnal} + DHI_{diurnal}) A_{PV}}$, and $\eta_{operating}$ was defined as $\frac{LVH_{H_2} m_{H_2}}{(DNI_{operating} + DHI_{operating}) A_{PV}}$, in which LVH_{H_2} is the lower heating value of hydrogen, m_{H_2} the mass of hydrogen collected from the vanadium discharge reaction, and A_{PV} the area of the photovoltaic module; $DNI_{diurnal}$ and $DNI_{operating}$ are the direct normal irradiance integrated over a diurnal cycle and operating cycle, respectively; and $DHI_{dirunal}$ and $DHI_{operating}$ are the direct horizontal irradiance integrated over a diurnal cycle and operating cycle, respectively. By collecting the produced $H_2(g)$ at night, $\eta_{diurnal}$ = 3.7% and $\eta_{operating}$ = 5.8% were obtained. PV modules with higher conversion efficiencies can further improve the overall efficiency of this hybrid device, provided that the operating voltage of the module is ∼2.2−2.3 V, to maintain the desired cathode operating potential.

While the demonstration unit contained two discrete components, a PV cell and an electrochemical reactor with the dark electrodes operating at current densities relevant to the solar photon flux, a fully integrated hybrid device can be envisioned and constructed using many of the design principles in integrated PEC water-splitting reactors.[38,39] The further development and potential deployment of such hybrid devices will likely primarily be in distributed applications and in places where electric grids and electrical transmission are not available. In the distributed applications, the operating current density of the catalysts and dark electrodes will be ∼10 mA cm^{-2} as driven by unconcentrated sunlight; hence, the system described herein captures the key performance metrics and characteristics of such a device. In addition, the Mo_2C powder used in this study could be replaced with a high surface area, porous medium to eliminate the filtering process, and the required catalyst loading for the discharging process is relatively low for scalability of this concept. For instance, without any optimization of the Mo_2C loading, to completely discharge the vanadium electrolyte from a relatively large photoactive device (100 cm^2 active area, 10% STH conversion efficiency, 7 kWh/m^2/day solar insolation) under operation during the day, only 5 g of Mo_2C catalyst will be needed to generate the hydrogen within 30 min during the night.

In summary, a proof-of-concept, hybrid solar-driven water-splitting device was demonstrated that produces $O_2(g)$ in the daylight and produces $H_2(g)$ on demand at an elevated pressure. Instead of transporting high-pressure H_2 over a large area in a traditional solar-driven water-splitting device that produces H_2 and O_2 simultaneously under illumination, the bipolar membrane-based hybrid device stores the renewable electrons and protons temporarily (daily, weekly, or even seasonally) in the liquid form, e.g., vanadium-based redox couples, which can be transported readily into a centralized reactor for production of H_2 as desired. The "solar-charged" vanadium redox couples could also be used in parallel with short-term electricity storage in the grid or longer-term fuel production in conjunction with further reduction reactions, including CO_2 reduction or biomass upgrades. The approach is complementary to other approaches that are being developed to decouple the production of $H_2(g)$ and $O_2(g)$ in a water-splitting process, each of which has unique advantages and disadvantages from complexity, cost, and safety perspectives in laboratory-sized demonstration systems in their use of simple versus bipolar membranes, single versus dual electrochemical cells, earth-abundant versus precious metal electrocatalysts, etc. The hybrid device described herein thus provides additional possible design spaces for implementation of a hydrogen-based "solar refinery".

DOI: 10.1021/acsenergylett.9b00278
ACS Energy Lett. 2019, 4, 968−976

■ ASSOCIATED CONTENT

Supporting Information

The Supporting Information is available free of charge on the ACS Publications website at DOI: 10.1021/acsenergylett.9b00278.

Electrolyte and catalyst material information, electrochemical cell, electrochemical charging experiments, bipolar membrane measurement details, ion crossover measurements, outdoor charging experiments, and pressurization experiments (PDF)

■ AUTHOR INFORMATION

Corresponding Authors

*E-mail: nslewis@caltech.edu (N.S.L).
*E-mail: cxx@caltech.edu (C.X.).

ORCID

Lihao Han: 0000-0002-0452-3381
Chengxiang Xiang: 0000-0002-1698-6754

Notes

The authors declare no competing financial interest.

■ ACKNOWLEDGMENTS

This material is based upon work performed by the Joint Center for Artificial Photosynthesis, a DOE Energy Innovation Hub, supported through the Office of Science of the U.S. Department of Energy under Award Number DE-SC0004993, as well as the Gordon and Betty Moore Foundation. The authors thank Caltech's SURF Board for a Summer Undergraduate Research Fellowship and acknowledge Caltech's Federal Work-Study program.

■ REFERENCES

(1) Haynes, W. M.; Lide, D. R.; Bruno, T. J. *CRC Handbook of Chemistry and Physics: A Ready-Reference Book of Chemical and Physical Data*; CRC Press, Taylor & Francis Group: Boca Raton, FL, 2015.

(2) Verlage, E.; Hu, S.; Liu, R.; Jones, R. J. R.; Sun, K.; Xiang, C.; Lewis, N. S.; Atwater, H. A. A Monolithically Integrated, Intrinsically Safe, 10% Efficient, Solar-Driven Water-Splitting System Based on Active, Stable Earth-Abundant Electrocatalysts in Conjunction with Tandem Iii-V Light Absorbers Protected By Amorphous TiO_2 Films. *Energy Environ. Sci.* **2015**, *8* (11), 3166−3172.

(3) Sun, K.; Liu, R.; Chen, Y.; Verlage, E.; Lewis, N. S.; Xiang, C. A Stabilized, Intrinsically Safe, 10% Efficient, Solar-Driven Water-Splitting Cell Incorporating Earth-Abundant Electrocatalysts with Steady-State pH Gradients and Product Separation Enabled by a Bipolar Membrane. *Adv. Energy Mater.* **2016**, *6* (13), 1600379.

(4) Luo, J.; Vermaas, D. A.; Bi, D.; Hagfeldt, A.; Smith, W. A.; Grätzel, M. Bipolar Membrane-Assisted Solar Water Splitting in Optimal pH. *Adv. Energy Mater.* **2016**, *6*, 1600100.

(5) Luo, J.; Im, J.-H.; Mayer, M. T.; Schreier, M.; Nazeeruddin, M. K.; Park, N.-G.; Tilley, S. D.; Fan, H. J.; Grätzel, M. Water Photolysis at 12.3% Efficiency via Perovskite Photovoltaics and Earth-Abundant Catalysts. *Science* **2014**, *345* (6204), 1593−1596.

(6) Wrighton, M. S.; Ellis, A. B.; Wolczanski, P. T.; Morse, D. L.; Abrahamson, H. B.; Ginley, D. S. Strontium Titanate Photoelectrodes. Efficient Photoassisted Electrolysis of Water at Zero Applied Potential. *J. Am. Chem. Soc.* **1976**, *98* (10), 2774−2779.

(7) Najjar, Y. S. H. Hydrogen Safety: The Road toward Green Technology. *Int. J. Hydrogen Energy* **2013**, *38* (25), 10716−10728.

(8) Jin, J.; Walczak, K.; Singh, M. R.; Karp, C.; Lewis, N. S.; Xiang, C. An Experimental and Modeling/Simulation-Based Evaluation of the Efficiency and Operational Performance Characteristics of an Integrated, Membrane-Free, Neutral pH Solar-Driven Water-Splitting System. *Energy Environ. Sci.* **2014**, *7* (10), 3371−3380.

(9) H. Hashemi, S. M.; Modestino, M. A.; Psaltis, D. A Membrane-less Electrolyzer for Hydrogen Production across the pH Scale. *Energy Environ. Sci.* **2015**, *8* (7), 2003−2009.

(10) Hashemi, S. M. H.; Neuenschwander, M.; Hadikhani, P.; Modestino, M. A.; Psaltis, D. Membrane-less Micro Fuel Cell Based on Two-Phase Flow. *J. Power Sources* **2017**, *348*, 212−218.

(11) Rohland, B.; Eberle, K.; Ströbel, R.; Scholta, J.; Garche, J. Electrochemical Hydrogen Compressor. *Electrochim. Acta* **1998**, *43* (24), 3841−3846.

(12) Ströbel, R.; Oszcipok, M.; Fasil, M.; Rohland, B.; Jörissen, L.; Garche, J. The Compression of Hydrogen in an Electrochemical Cell Based on a PE Fuel Cell Design. *J. Power Sources* **2002**, *105* (2), 208−215.

(13) Collier, A.; Wang, H.; Zi Yuan, X.; Zhang, J.; Wilkinson, D. P. Degradation of Polymer Electrolyte Membranes. *Int. J. Hydrogen Energy* **2006**, *31* (13), 1838−1854.

(14) Tang, H.; Peikang, S.; Jiang, S. P.; Wang, F.; Pan, M. A Degradation Study of Nafion Proton Exchange Membrane of PEM Fuel Cells. *J. Power Sources* **2007**, *170* (1), 85−92.

(15) Chen, L.; Dong, X.; Wang, Y.; Xia, Y. Separating Hydrogen and Oxygen Evolution in Alkaline Water Electrolysis Using Nickel Hydroxide. *Nat. Commun.* **2016**, *7*, 11741.

(16) Landman, A.; Dotan, H.; Shter, G. E.; Wullenkord, M.; Houaijia, A.; Maljusch, A.; Grader, G. S.; Rothschild, A. Photoelectrochemical Water Splitting in Separate Oxygen and Hydrogen Cells. *Nat. Mater.* **2017**, *16*, 646−651.

(17) Ma, Y. Y.; Dong, X. L.; Wang, Y. G.; Xia, Y. Y. Decoupling Hydrogen and Oxygen Production in Acidic Water Electrolysis Using a Polytriphenylamine-Based Battery Electrode. *Angew. Chem., Int. Ed.* **2018**, *57* (11), 2904−2908.

(18) Bloor, L. G.; Solarska, R.; Bienkowski, K.; Kulesza, P. J.; Augustynski, J.; Symes, M. D.; Cronin, L. Solar-Driven Water Oxidation and Decoupled Hydrogen Production Mediated by an Electron-Coupled-Proton Buffer. *J. Am. Chem. Soc.* **2016**, *138* (21), 6707−6710.

(19) Symes, M. D.; Cronin, L. Decoupling Hydrogen and Oxygen Evolution during Electrolytic Water Splitting Using an Electron-Coupled-Proton Buffer. *Nat. Chem.* **2013**, *5* (5), 403−409.

(20) Rausch, B.; Symes, M. D.; Chisholm, G.; Cronin, L. Decoupled Catalytic Hydrogen Evolution from a Molecular Metal Oxide Redox Mediator in Water Splitting. *Science* **2014**, *345* (6202), 1326−1330.

(21) Amstutz, V.; Toghill, K. E.; Powlesland, F.; Vrubel, H.; Comninellis, C.; Hu, X. L.; Girault, H. H. Renewable Hydrogen Generation from a Dual-Circuit Redox Flow Battery. *Energy Environ. Sci.* **2014**, *7* (7), 2350−2358.

(22) McCrory, C. C. L.; Jung, S.; Ferrer, I. M.; Chatman, S. M.; Peters, J. C.; Jaramillo, T. F. Benchmarking Hydrogen Evolving Reaction and Oxygen Evolving Reaction Electrocatalysts for Solar Water Splitting Devices. *J. Am. Chem. Soc.* **2015**, *137* (13), 4347−4357.

(23) McCrory, C. C. L.; Jung, S.; Peters, J. C.; Jaramillo, T. F. Benchmarking Heterogeneous Electrocatalysts for the Oxygen Evolution Reaction. *J. Am. Chem. Soc.* **2013**, *135* (45), 16977−16987.

(24) Sun, K.; Saadi, F. H.; Lichterman, M. F.; Hale, W. G.; Wang, H.-P.; Zhou, X.; Plymale, N. T.; Omelchenko, S. T.; He, J.-H.; Papadantonakis, K. M.; et al. Stable Solar-Driven Oxidation of Water by Semiconducting Photoanodes Protected by Transparent Catalytic Nickel Oxide Films. *Proc. Natl. Acad. Sci. U. S. A.* **2015**, *112* (12), 3612−3617.

(25) Sun, K.; McDowell, M. T.; Nielander, A. C.; Hu, S.; Shaner, M. R.; Yang, F.; Brunschwig, B. S.; Lewis, N. S. Stable Solar-Driven Water Oxidation to O_2(g) by Ni-Oxide-Coated Silicon Photoanodes. *J. Phys. Chem. Lett.* **2015**, *6* (4), 592−598.

(26) Zhou, X.; Liu, R.; Sun, K.; Friedrich, D.; McDowell, M. T.; Yang, F.; Omelchenko, S. T.; Saadi, F. H.; Nielander, A. C.; Yalamanchili, S.; et al. Interface Engineering of the Photoelectrochemical Performance of Ni-Oxide-Coated n-Si Photoanodes by Atomic-Layer Deposition of Ultrathin Films of Cobalt Oxide. *Energy Environ. Sci.* **2015**, *8* (9), 2644−2649.

(27) Kenney, M. J.; Gong, M.; Li, Y.; Wu, J. Z.; Feng, J.; Lanza, M.; Dai, H. High-Performance Silicon Photoanodes Passivated with

DOI: 10.1021/acsenergylett.9b00278
ACS Energy Lett. 2019, 4, 968−976

Ultrathin Nickel Films for Water Oxidation. *Science* **2013**, *342* (6160), 836−40.
(28) Walter, M. G.; Warren, E. L.; McKone, J. R.; Boettcher, S. W.; Mi, Q.; Santori, E. A.; Lewis, N. S. Solar Water Splitting Cells. *Chem. Rev.* **2010**, *110* (11), 6446−6473.
(29) Jiang, C.; Moniz, S. J. A.; Wang, A.; Zhang, T.; Tang, J. Photoelectrochemical Devices for Solar Water Splitting - Materials and Challenges. *Chem. Soc. Rev.* **2017**, *46* (15), 4645−4660.
(30) Sivula, K.; van de Krol, R. Semiconducting Materials for Photoelectrochemical Energy Conversion. *Nat. Rev. Mater.* **2016**, *1*, 15010.
(31) Heller, A.; Miller, B.; Thiel, F. A. 11.5% Solar Conversion Efficiency in the Photocathodically Protected *p*-InP/V^{3+}-V^{2+}-HCl/C Semiconductor Liquid Junction Cell. *Appl. Phys. Lett.* **1981**, *38* (4), 282−284.
(32) Reiter, R. S.; White, W.; Ardo, S. Communication—Electrochemical Characterization of Commercial Bipolar Membranes under Electrolyte Conditions Relevant to Solar Fuels Technologies. *J. Electrochem. Soc.* **2016**, *163* (4), H3132−H3134.
(33) Vermaas, D. A.; Wiegman, S.; Nagaki, T.; Smith, W. A. Ion Transport Mechanisms in Bipolar Membranes for (Photo)-electrochemical Water Splitting. *Sustainable Energy Fuels* **2018**, *2* (9), 2006−2015.
(34) Vargas-Barbosa, N. M.; Geise, G. M.; Hickner, M. A.; Mallouk, T. E. Assessing the Utility of Bipolar Membranes for use in Photoelectrochemical Water-Splitting Cells. *ChemSusChem* **2014**, *7* (11), 3017−3020.
(35) Zhou, X.; Liu, R.; Sun, K.; Chen, Y.; Verlage, E.; Francis, S. A.; Lewis, N. S.; Xiang, C. Solar-Driven Reduction of 1 atm of CO_2 to Formate at 10% Energy-Conversion Efficiency by Use of a TiO_2-Protected III−V Tandem Photoanode in Conjunction with a Bipolar Membrane and a Pd/C Cathode. *ACS Energy Lett.* **2016**, *1* (4), 764−770.
(36) Yan, Z.; Zhu, L.; Li, Y. C.; Wycisk, R. J.; Pintauro, P. N.; Hickner, M. A.; Mallouk, T. E. The Balance of Electric Field and Interfacial Catalysis in Promoting Water Dissociation in Bipolar Membranes. *Energy Environ. Sci.* **2018**, *11* (8), 2235−2245.
(37) Vermaas, D. A.; Sassenburg, M.; Smith, W. A. Photo-Assisted Water Splitting with Bipolar Membrane Induced pH Gradients for Practical Solar Fuel Devices. *J. Mater. Chem. A* **2015**, *3* (38), 19556−19562.
(38) Haussener, S.; Xiang, C. X.; Spurgeon, J. M.; Ardo, S.; Lewis, N. S.; Weber, A. Z. Modeling, Simulation, and Design Criteria for Photoelectrochemical Water-Splitting Systems. *Energy Environ. Sci.* **2012**, *5* (12), 9922−9935.
(39) Xiang, C.; Weber, A. Z.; Ardo, S.; Berger, A.; Chen, Y.; Coridan, R.; Fountaine, K. T.; Haussener, S.; Hu, S.; Liu, R.; et al. Modeling, Simulation, and Implementation of Solar-Driven Water-Splitting Devices. *Angew. Chem., Int. Ed.* **2016**, *55* (42), 12974−12988.
(40) Saadi, F. H.; Carim, A. I.; Drisdell, W. S.; Gul, S.; Baricuatro, J. H.; Yano, J.; Soriaga, M. P.; Lewis, N. S. Operando Spectroscopic Analysis of CoP Films Electrocatalyzing the Hydrogen-Evolution Reaction. *J. Am. Chem. Soc.* **2017**, *139* (37), 12927−12930.
(41) Saadi, F. H.; Carim, A. I.; Verlage, E.; Hemminger, J. C.; Lewis, N. S.; Soriaga, M. P. CoP as an Acid-Stable Active Electrocatalyst for the Hydrogen-Evolution Reaction: Electrochemical Synthesis, Interfacial Characterization and Performance Evaluation. *J. Phys. Chem. C* **2014**, *118* (50), 29294−29300.

DOI: 10.1021/acsenergylett.9b00278
ACS Energy Lett. 2019, 4, 968−976